Published online November 20, 2007

Vadose Zone Journal ORIGINAL RESEARCH

Elucidation of Flow and Transport Processes in a Variably Saturated System of Interlayered Sediment and Fractured Rock Using Tracer Tests

Catherine L. Duke,* Robert C. Roback, Paul W. Reimus, Robert S. Bowman, Travis L. McLing, Kristine E. Baker, and Larry C. Hull

The objective of this work was to investigate flow and transport in a layered, variably saturated system consisting of both fractured rock and sedimentary material during focused infiltration from the surface. Two tracer tests were performed using the Vadose Zone Research Park (VZRP) at the Idaho National Laboratory (INL). The first test occurred under quasi-steady-state conditions and the second was initiated in a much drier system and thus provided information regarding flow and transport under transient conditions. A one-dimensional analytical model was used to fit breakthrough curves resulting from the two tracer tests. The results of this modeling provide insight into the nature of flow in the fractured basalt, surficial alluvium, and sedimentary interbeds that comprise the vadose zone of the eastern Snake River Plain. Flow through the fractured basalt is focused and preferential in nature, and multiple flow paths arise due to numerous fractures functioning as transmissive pathways in addition to flow splitting along geologic contacts. Flow velocities were significantly higher during the test with the wetter flow domain, presumably due to increases in hydraulic conductivity associated with higher water contents of the geologic materials. Perching was observed above the alluvium–basalt contact and above the lower boundary of a locally continuous sedimentary interbed. The perching behavior between the two contacts was fundamentally different; the perched layer above the alluvium–basalt contact was neither laterally extensive nor temporally persistent in the absence of infiltration from the surface. In contrast, the perched layer along the interbed was significantly thicker and gave rise to lateral flow over distances on the order of hundreds of meters. Vertical transport is shown to occur predominantly through the main bulk of the sedimentary material of the interbed; lateral flow appears to occur primarily in the fractured basalt directly above the interbed.

ABBREVIATIONS: 1-D ADE, one-dimensional advection–dispersion equation; 2,4-DFBA, 2,4-difluorobenzoate; 2,4,5-TFBA, 2,4,5-trifluorobenzoate; bls, below land surface; BTC, breakthrough curve; ESRP, eastern Snake River Plain; FBA, fluorobenzoate; INL, Idaho National Laboratory; INTEC, Idaho Nuclear Technology and Engineering Center; LSIT, Large Scale Infiltration Test; QL, quantification limit; RWMC, Radioactive Waste Management Complex; VZRP, Vadose Zone Research Park.

Understanding flow and transport in variably saturated, layered and fractured geologic systems is critically important for managing waste disposal and determining remediation strategies. For many contaminated sites, the vadose zone is the only barrier between the source of contamination and the regional aquifer. Repositories for radioactive and hazardous wastes have been proposed in unsaturated, fractured rock that is expected to prevent contaminant release to the accessible environment. For many years, it was thought that highly negative pressures within the unsaturated matrix of fractured rocks would prevent flow from occurring in the fractures until the surrounding matrix was saturated or close to saturated (Montazer and Wilson, 1984; Wang and Narasimhan, 1985, 1993; Peters and Klavetter, 1988). Thus, flow was expected to proceed at relatively low rates that could be predicted using Richard's equation–type formulations. Growing evidence from both field experiments and numerical modeling efforts, however, has shown that substantial flow does occur in fractures surrounded by unsaturated matrix (Fabryka-Martin et al., 1993, 1994; Faybishenko et al., 2000; Finsterle et al., 2002; Flint et al., 2001b; Gauthier et al., 1992; Illman and Hughson, 2005; Liu et al., 1998; Yang et al., 1996). This flow mechanism appears to be especially important during unsaturated flow associated with intense, episodic infiltration events (McLaren et al., 2000; Pruess, 1999). Fracture flow in unsaturated media gives rise to much faster contaminant travel times and lower effective sorption than would be predicted based on a matrix-flow conceptual model.

In deep vadose zones, contacts between units of differing hydrogeologic characteristics (fractured vs. unfractured, consolidated vs. unconsolidated) have important implications for flow distribution (e.g., Adam et al., 2004; Flint et al., 2001a; Nimmo et al., 2004b; Robinson et al., 2005). Issues associated with such contacts include the formation of perched aquifers, interruption of vertical flow, and lateral diversion of infiltrating water. Perched aquifers may store significant amounts of water within the vadose zone and, as such, may act as reservoirs within which contaminants are either concentrated or diluted (Nimmo et al., 2004b). Lateral redistribution of water may serve to limit infiltration through a waste site or repository horizon but can also act to divert polluted water to preferential pathways such as fault zones that provide fast paths to the regional aquifer (Flint et al., 2001a). Whether lateral flow occurs above or within an imped-

C.L. Duke, Errol L. Montgomery & Associates, Inc., 1550 E. Prince Rd., Tucson, AZ 85719; R.C. Roback and P.W. Reimus, Earth and Environmental Science Division, MS J514, Los Alamos National Lab., Los Alamos, NM 87545; R.S. Bowman, Dep. Earth and Environmental Science, New Mexico Institute of Mining and Technology, 801 Leroy Pl., Socorro, NM 87801; T.L. McLing, K.E. Baker, and L.C. Hull, Geosciences, Idaho National Lab., P.O. Box 1625, Idaho Falls, ID 83415. Received 19 July 2006. *Corresponding author (kduke@elmontgomery.com).

Vadose Zone J. 6:855–867
doi:10.2136/vzj2006.0102

ing layer has important implications for the rate at which flow may be expected to occur. In addition, the potential for sorption and other physicochemical interaction between dissolved solutes and the rock will vary depending on the unit through which the solutes are being transported.

Radionuclide contamination in the vadose zone, and the potential for contaminant migration to the aquifer, is one of the most serious environmental concerns at Idaho National Laboratory (INL). At the Radioactive Waste Management Complex (RWMC), low-level radioactive wastes were buried in near-surface pits and trenches. At the Idaho Nuclear Technology and Engineering Center (INTEC, formerly the Idaho Chemical Processing Plant), spills and leaks from transfer lines have resulted in contamination of near-surface sediments as well as of perched water bodies deeper in the vadose zone. To predict the behavior of such contamination, we must understand the nature of flow in the vadose zone, particularly fracture–matrix interactions and the role of geologic contacts and the associated perched zones of saturation.

Over the past couple of decades, long-term monitoring, field-scale experiments, and associated modeling efforts have been performed at INL. Three tracer tests were performed in the 1990s: the Large Scale Infiltration Test (LSIT), the Box Canyon tests, and the Spreading Area test (these tests are described in detail below). The goal of these studies was to reduce uncertainty in the conceptual understanding of flow and transport in this very complex hydrogeological setting as well as to provide site-specific transport parameters that could be used in risk assessment (Doughty, 2000; Dunnivant et al., 1998, 1995; Faybishenko et al., 2000; Magnuson, 1995, 2004; Mattson et al., 2004; Nimmo et al., 2002; Wood and Norrell, 1996). A relatively robust conceptual model has resulted from this work, but several issues require further clarification. The effects of transient infiltration events and antecedent wetness on flow velocities (and therefore residence times in each geologic unit) have not been defined. In addition, understanding of perching mechanisms and the persistence and lateral extent of the resulting saturated layers is lacking. Although lateral flow is known to be associated with sedimentary interbeds, it is not clear whether this flow occurs in the sedimentary material of the interbeds themselves or in the high-permeability basalt rubble zones with which the interbeds are often associated (Nimmo et al., 2004b). It is also unclear to what degree water bypasses the highly sorptive sedimentary materials of the interbeds due to flow mechanisms such as instability-linked flow fingering and funneling within the sediments or by accessing preferential flow paths through discontinuities in the interbed.

To address these issues and further clarify the behavior of this system during high-flux infiltration from the surface, we performed two tracer tests using the Vadose Zone Research Park (VZRP) at INL. Tracers were applied in two infiltration ponds and were sampled at three depths: at the base of the surficial alluvium where it contacts fractured basalt, within a laterally continuous and relatively thick sedimentary interbed (the CD interbed), and at the interface between the fractured basalt and the top of the CD interbed. The first tracer test was performed under relatively wet, quasi-steady-state hydrologic conditions; the second test investigated transport during infiltration into an initially dry system.

Both tracer tests yielded valuable information for INL as well as other sites with similar hydrogeologic systems in that (i) they were performed at a scale of 100s of meters, which is directly relevant to questions regarding transport at the site and facility scale, (ii) they investigated flow in the fractured basalt, in the surficial alluvium and in the interbed sediments, as well as at the contacts between these units, and (iii) they simulated episodic infiltration events on two temporal scales that are of concern at INL and in other semiarid environments subject to both short-term, seasonal flooding (days–weeks) and longer-duration floods of several months. Analysis of tracer test results facilitated by the use of a simple one-dimensional transport model provided insight into the nature of flow in each of the geologic units of concern and allowed comparison of transport behavior between units under differing infiltration conditions.

Hydrogeology of the Eastern Snake River Plain

The Idaho National Laboratory occupies approximately 2300 km^2 of the eastern Snake River Plain (ESRP) in southeast Idaho (Fig. 1). Underlying the plain is the Snake River Plain aquifer that provides agricultural and domestic water to much of southeastern Idaho. The vadose zone is approximately 60 m deep at the northern border of INL and thickens to about 200 m at the southern border. The ESRP hosts a thick sequence of Tertiary and Quaternary pahoehoe basalt flows that erupted from small shield volcanoes (Schaefer and Kattenhorn, 2004; Smith, 2004). Individual lava flows are low volume (0.005–7 km^3) and have a fairly consistent and well-defined internal structure. Schaefer and Kattenhorn (2004) described a typical basalt flow as having an upper and lower colonnade separated by a densely fractured entablature. Fractures in the upper colonnade are more closely spaced than those in the lower colonnade and are both column-bounding and column-normal. In contrast, the lower colonnade is distinguished by more sparsely distributed

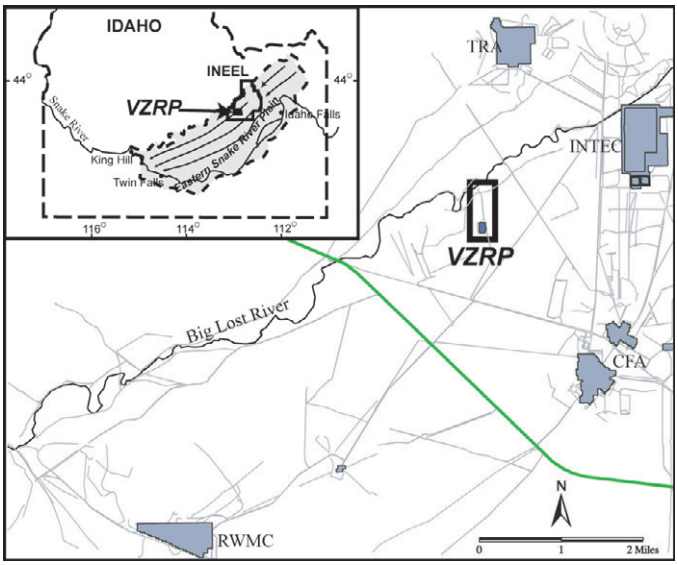

FIG. 1. Location of Vadose Zone Research Park (VZRP) and nearby facilities, the Radioactive Waste Management Complex (RWMC), Idaho Nuclear Technology and Engineering Center (INTEC), Test Reactor Area (TRA), and Central Facilities Area (CFA). Arrows in the inset indicate the direction of regional groundwater flow.

fractures that are primarily column-bounding. The entablature, although intensely fractured, contains few column-bounding fractures and in fact serves to prevent column-bounding fractures from the upper and lower colonnades connecting across the flow. Schaefer and Kattenhorn (2004) noted that entablatures were not present in all the flows that they studied. This observation was supported by Faybishenko et al. (2000), who observed densely fractured, subhorizontal central zones in ~40% of the flows examined at their Box Canyon experimental site located in the eastern Snake River Plain adjacent to INL. Schaefer and Kattenhorn (2004) suggested that column-bounding fractures are likely the features of greatest significance in controlling hydraulic conductivity within a single basalt flow as they are the longest and most-connected fractures and have the greatest apertures. This idea is supported by the fact that column-bounding fractures are often lined with secondary minerals, whereas entablature fractures generally are not. Faybishenko et al. (2000) also identified vertical to subvertical column-bounding fractures as the predominant flow pathway through individual basalt flows exposed at Box Canyon.

During periods of volcanic quiescence, sedimentary materials consisting of lacustrine deposits, alluvial material, and aeolian sediments have been deposited in the topographic lows between the basalt flows. These now form laterally discontinuous sedimentary interbeds, which, in turn, are overlain by the next generation of basalt flows (Anderson and Lewis, 1989; Barraclough et al., 1976; Schaefer and Kattenhorn, 2004; Smith, 2004).

The margins of basalt flows are commonly highly fractured and rubbly, giving rise to high-permeability zones of rubble, fractures, and clinker collectively known as either rubble zones (Nimmo et al., 2004b; Smith, 2004) or interflow zones (Ackerman, 1991). Rubble zones are found between 5 and 20% of the basalt flows and have hydraulic conductivities on the order of 800 m d^{-1} or higher (Nimmo et al., 2004b). Rubble zones in contact with a low-permeability feature such as massive basalt or a sedimentary interbed may host significant perched aquifers and facilitate lateral flow for distances on the order of 100s to 1000s of meters (Nimmo et al., 2002). Nimmo et al. (2004b) pointed out that observed rapid lateral transport rates over distances of 1000 m or more indicate that rubble zones may exhibit large-scale continuity under some conditions.

Conceptual Model of Flow and Transport in the Eastern Snake River Plain Vadose Zone

Over the past 10 yr, three tracer tests of note have been performed in the variably saturated, fractured basalt and interlayered sediments of the ESRP. In chronological order, these consist of the LSIT performed in 1994 (Newman and Dunnivant, 1995; Wood and Norrell, 1996), the Box Canyon tests performed in 1996 and 1997 (Doughty, 2000; Faybishenko et al., 2000), and the Spreading Area test performed in 1999 (Nimmo et al., 2002). Each of these tests was intended to investigate flow and transport in the vadose zone of the ESRP at a different scale. The LSIT provided information on the 100s of meters scale, the Box Canyon tests concentrated on flow and transport within a single basalt flow (scale of several meters) and the Spreading Area test provided information on the 100s to 1000s of meters scale.

The LSIT was performed in a 26,000-m^2 infiltration pond at the RWMC at INL (see Fig. 1 for location of the RWMC). The pond was flooded for 6 d, and then a conservative tracer, Se-75, was added to the pond, after which flow was continued for another 30 d. One hundred and one monitoring wells and lysimeters were installed in and around the pond in three concentric rings. Water was collected at 30 of the 101 monitoring points, and tracer was detected at 26 of these sites. No water was recovered from any well or lysimeter outside the footprint of the pond except at a depth of 70 m, where a sedimentary interbed caused perching and lateral flow. One of the most important findings of this test was that infiltration through the unsaturated basalt is essentially vertical until intercepted by an interbed, at which point perching and lateral flow occur. In addition, application of the one-dimensional advection–dispersion equation to breakthrough data from the LSIT provided estimates of flow velocity (v) and longitudinal dispersivity (α) for the unsaturated basalt (mean v = 1.01 m d^{-1}; range of α = 0.18–3.92 m) and along the interbed (mean v = 5.02 m d^{-1}; range of α = 0.10–45.80 m) (Dunnivant et al., 1998).

Faybishenko et al. (2000) performed five infiltration tracer tests at Box Canyon near INL in 1996 and 1997. These were relatively short duration tests (2 d to 2 wk) designed to explore flow and transport within a single basalt flow. Faybishenko et al. (2000) concluded from the location of tracer detections that solutes moved rapidly through preferential flow pathways. They identified column-bounding fractures as the primary conduit for flow between the surface and the lower boundary of the basalt flow under investigation. The authors concluded that water flowed rapidly through saturated fractures and that the surrounding matrix saturated slowly (on the order of days) as long as there was water in the fracture. Finally, they pointed out that some fractures that were initially wet drained after the beginning of the test, even though infiltration from the surface had reached a steady rate. The conceptual model of Faybishenko et al. (2000) identified a variety of mass transport mechanisms based both on geology and on distribution of saturation. These mechanisms include (i) fracture-to-matrix diffusion, (ii) vesicular basalt-to-massive basalt diffusion, (iii) preferential flow through conductive fractures and the effect of funneling, (iv) vesicular basalt-to-nonconductive fracture diffusion, (v) conductive fracture-to-vesicular basalt flow and diffusion, (vi) lateral flow and advective transport in the central fracture zone, (vii) lateral flow and advective transport in the rubble zone, and (viii) flow into the underlying basalt (see Fig. 17 in Faybishenko et al., 2000).

The Spreading Area test of Nimmo et al. (2002) was conducted using large flood control ponds located ~10 km upstream of the VZRP on the Big Lost River at INL. Nimmo et al. (2002) placed 675 kg of the conservative tracer 1,5-naphthalene disulfonate into two flooded spreading areas. A network of monitoring wells was used to sample water from perched zones 100s to 1000s of meters from the spreading areas. Tracer recovery results indicated that within 9 d, water moved from the spreading areas vertically to the aquifer. In less than 4 mo, tracer was transported laterally along perched layers for distances up to 1.3 km. From these observations, the authors concluded that although low-permeability layers divert water laterally, they do not prevent solute transport to the aquifer. They also noted that horizontal flow probably occurs under essentially saturated conditions at rates

as high as 14 m d^{-1}. In a follow-up study Nimmo et al. (2004a) proposed that horizontal flow through saturated high-permeability zones in the basalt associated with laterally continuous interbeds may be described as Darcian flow.

Based on the three studies outlined above, together with data from long-term monitoring at INL (Anderson and Lewis, 1989; Barraclough et al., 1976; Mattson et al., 2004; Rightmire and Lewis, 1987), a conceptual model has been developed. The model has seven major components:

1. Water moves mostly vertically through the basalt until it reaches a geologic contact or other area of strong permeability contrast that diverts water laterally.
2. Percolation through the fractured basalt occurs primarily in column-bounding fractures; however, these fractures do not necessarily remain wet but rather fill and empty with time even when infiltration has reached a steady rate.
3. During percolation through a previously dry subsurface, the basalt matrix is initially unsaturated but saturates gradually as long as the bounding fractures contain water.
4. Diffusive mass transport between mobile and immobile fluid domains is thought to be an important transport mechanism in the fractured basalt, but matrix diffusion has not been quantified.
5. Sedimentary interbeds act to slow downward flow, causing perched saturated zones and lateral flow.
6. Under saturated or near-saturated conditions, flow along the interbeds is facilitated by the combination of a low-permeability layer (the sediments of the interbed and clay-rich fracture fill in the associated basalt) overlain by a high-permeability basalt rubble zone that acts to conduct water laterally. Flow is thought to take place through the rubble zone under saturated or nearly saturated conditions.
7. Although the interbeds divert flow laterally, water and solutes eventually move downward. An important outstanding question is whether water moves through the sedimentary interbeds primarily through the matrix or via preferential flow paths.

Materials and Methods

Description of the Vadose Zone Research Park

The VZRP is a 2.6-km^2 (1 square mile) facility located in the southwestern portion of INL along the Big Lost River. The Big Lost River is an intermittent stream that flows from the Pioneer Mountains to the west, enters INL, and then turns north to a series of sinks and playas where it terminates. A network of monitoring wells and instrumented boreholes surrounds two percolation ponds and extends some 1000 m north to the Big Lost River. The two roughly square percolation ponds are immediately adjacent to one another, and each measures approximately 76 m on an edge (Fig. 2). The primary function of the ponds is to dispose of uncontaminated wastewater generated by INTEC, which lies approximately 4 km to the northeast of the VZRP. The INTEC diverts an average of 3800 to 5700 m^3 ($\sim 1.0 \times 10^6$ to 1.5×10^6 gal.) of water to one or the other of the ponds daily. This water is pumped from an aquifer well near the INTEC, softened using an ion exchange resin, and circulated through the facility before disposal at the VZRP.

At the VZRP (Fig. 3), the surficial alluvium is approximately 15 m thick and consists of alluvial gravels, pebbles, and cobbles mixed with fine-grained silty and clayey sand (Smith, 2004). Below the surficial alluvium lie multiple layers of basalt and interbedded sediments. The monitoring network at the VZRP is focused largely within the 25 m of basalt that lies between the alluvium and a sedimentary interbed at approximately 40 m depth. This interbed is relatively continuous beneath the VZRP, has an average thickness of ~5 m, and is known as the CD interbed because it lies between the C and D basalt units (Baker et al., 2004). Although the alluvium–basalt contact and the contact between the basalt and the CD interbed are the focus of this study, inspection of the well logs from the VZRP indicates that many smaller, less-continuous sediment and clay layers and lenses are interspersed throughout the basalt. The hydrogeology of the VZRP is representative of the vadose zone throughout INL and the ESRP. As a result, although this study was performed on a local scale, the results are applicable to the much larger, regional scale. Furthermore, the hydrogeologic setting of a thick vadose zone with layers of geologic material of strongly contrasting permeabilities is typical of many arid and semiarid regions.

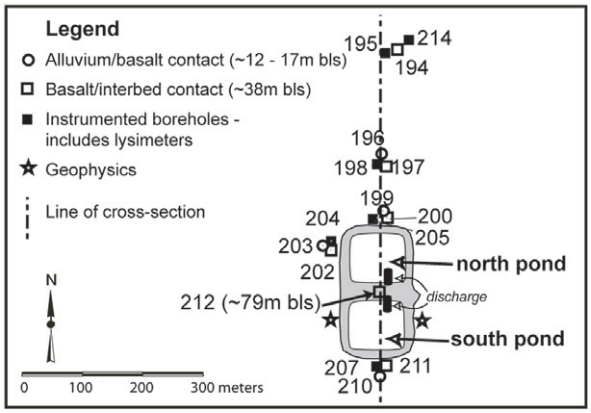

FIG. 2. Map of infiltration ponds and associated near-field monitoring network at the Vadose Zone Research Park.

Thirty-nine wells and instrumented boreholes are located around the percolation ponds and in a line northward to the Big Lost River. Wells and boreholes are distributed in nested sets (Fig. 2 and 3). Each set consists of a shallow monitoring well completed at the alluvium–basalt contact (~15–20 m below land surface [bls]), a deeper monitoring well completed at the

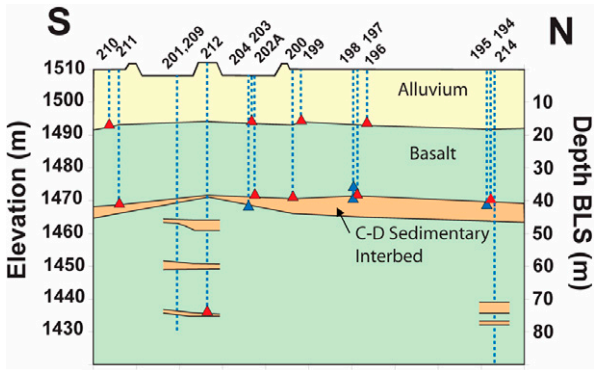

FIG. 3. Schematic cross-section showing lithology and monitoring network along the line of section of the Vadose Zone Research Park shown in Fig. 2. Wells 202, 203(A), and 204 are projected into the line of section. Red symbols represent monitoring wells; blue symbols represent suction lysimeters.

CD interbed (~40 m bls), and an instrumented borehole containing tensiometers, suction lysimeters, gas ports, water content sensors, and thermocouples located at various depths. In this paper each well or lysimeter identifier is followed by a letter in parentheses to indicate where the well is completed or the lysimeter is located. The letter (A) is for wells at the base of the alluvium, (B) for the lysimeter that is finished in the basalt and the wells at the contact between the basalt and the CD interbed, and (I) for suction lysimeters within the CD interbed. Well 202 collapsed during drilling, and a second hole was drilled and named well 202A; we refer to this well as well 202A(B). Identifiers of all other wells and lysimeters consist only of the relevant number and a letter in parentheses [e.g., well 210(A), well 211(B), and lysimeter 204129(I)].

Before infiltration from the ponds, the subsurface below the VZRP was relatively dry with only a few areas of local saturation. Initial moisture content analyses were performed at the USGS Unsaturated-Zone Flow laboratory in Menlo Park, CA (Winfield, 2003). Moisture content was determined gravimetrically on 10 interbed sediment samples taken from seven boreholes at depths ranging from ~40 to ~60 m. The majority of the samples were less than 50% saturated (volumetric water content < 0.2), an exception being two saturated samples collected from the CD interbed (Winfield, 2002). Similarly, the basalt was largely unsaturated although locally perched water occurred both within the basalt and at the contact between the basalt and the CD interbed (Baker et al., 2004). To test the water delivery system between INTEC and the VZRP, approximately 10,000 m^3 of water were discharged between 18 and 27 June 2002. About 10% of this water was released to the north pond, and the remainder to the south pond. High-volume discharge (~3800–5700 m^3 d^{-1}) began in the south pond on 27 Aug. 2002, switched to the north pond 21 Sept. 2002, and then back to the south pond 5 Oct. 2002. The discharge continued to the south pond until 31 June 2003 and was then switched to the north pond coincident with the start of the second tracer test of this study (Baker et al., 2004). While we did not quantify the initial spatial distribution of moisture beneath the north pond at the start of the second tracer test, there clearly would have been a decaying south-to-north lateral gradient in both the alluvium and the basalt due to infiltration from the south pond. This gradient could have initially diverted tracers to the north more than they otherwise would have been if there had not been an initial water mound beneath the south pond. We know, however, that saturated conditions did not exist at the base of the alluvium on the north side of the north pond during infiltration into the south pond, and we also know that the mound in the alluvium beneath the south pond decayed in ~4 d. Perched water levels at the base of the basalt never exceeded ~5.5 m at the periphery of the south pond [in well 211(B)], so the majority of the basalt thickness beneath the south pond remained unsaturated. Thus, the residual effects from the south pond infiltration on test 2 were limited both spatially and temporally.

Field Experiments to Characterize Water and Solute Movement

Two tracer tests were performed at the VZRP in summer 2003. The first was conducted in the south pond starting 11 June 2003. At this time the INTEC had been discharging water to the south pond for approximately 9 mo. Local areas of saturation were present at the southern end of the alluvium–basalt contact, but to the north and west the contact was unsaturated. Water was also perched along the CD interbed with water levels between 3.0 and 5.5 m above the upper surface of the CD interbed at the location of the wells. Based on water-level data from the wells, the flow system was considered to be at quasi–steady state. Maximum water-level fluctuations were on the order of 0.04 m d^{-1} and could be related to changes in the rate at which water was being discharged to the pond. Approximately 18.25 kg of 2,4,5-trifluorobenzoate (2,4,5-TFBA) was used as a conservative tracer. The 2,4,5-TFBA was "injected" by emptying tracer-containing carboys into the inflow of the south pond. For 2 h subsequent to the injection, grab samples were collected every 15 min at four locations around the pond.

The second tracer test differed fundamentally from the first test in that the system was relatively dry before the beginning of the test. Test 2 was conducted in the north pond, which had not received discharge water for 9 mo except for 14 d between 21 Sept. 2002 and 5 Oct. 2002. Two conservative tracers were used in this test; bromide ion (Br^-) and 2,4-difluorobenzoate (2,4-DFBA). The tracers (16.8 kg Br and 21.6 kg 2,4-DFBA) were mixed in a tank (~1600 L), which was located on the berm between the two ponds. On 31 July 2003, the discharge was switched from the south pond to the north pond, and the tracer mixture was added with the first water into a shallow pit in the floor of the north pond. The tracer was chased by continuous discharge to the north pond for the next several months.

After the first tracer addition (test 1), all the wells and lysimeters that yielded water were sampled every 2 to 4 h for 2 wk. The test 2 sampling period was longer, with samples collected every 3 to 4 h for a month and then less frequently for several more months. The characteristics of the wells and lysimeters that received water and were sampled during the two tracer tests are summarized in Table 1 (see Fig. 2 and 3 for locations). If possible, the wells were purged of 3 bore volumes before sampling.

TABLE 1. Descriptions of wells and lysimeters that received water during tests 1 and 2. Well and lysimeter numbers correspond with locations shown in Fig. 2 and 3. Letters in parentheses indicate where a well is completed or a lysimeter is located: A = alluvium–basalt contact, B = basalt–interbed contact, and I = within the CD interbed. Well 212 is a deeper well and has no associated letter.

Well/lysimeter ID	Location	Radial distance from well 212	Completion depth below land surface	Completion lithology
		m		
Well 199(A)	N of north pond	142	15.5	alluvium–basalt contact
Well 203(A)	NW of north pond	120	15.8	alluvium–basalt contact
Well 210(A)	S of south pond	142	18.1	alluvium–basalt contact
Well 197(B)	Far N of north pond	215	38.1	top CD interbed
Well 200(B)	N of north pond	129	38.7	top CD interbed
Well 202A(B)	NW of north pond	107	37.4	top CD interbed
Well 211(B)	S of south pond	133	39.0	top CD interbed
Well 212	Between ponds	0	79.2	deep basalt–interbed
Lys 198114(B)	Far N of north pond	215	34.7	fractured basalt ~3 m above CD interbed
Lys 198126(I)	Far N of north pond	215	38.4	within CD interbed
Lys 204129(I)	NW of north pond	120	39.3	below CD interbed

Due to transient flow conditions during test 2, some wells were pumped to dryness before 3 bore volumes were obtained. When this happened, the wells were allowed to recover for 5 to 15 min and then sampled. The alluvial wells to the north and northwest of the north pond [199(A) and 203(A)] were dry at the beginning of test 2. These wells were bailed until enough water was present to allow pumping. Samples were filtered using a 0.45-μm in-line filter. Suction lysimeters were purged with argon to remove all the water present at each sampling cycle, and samples were filtered using 0.45-μm nylon syringe filters. Between sampling events, a vacuum tank at the surface was connected to each of the suction lysimeters via tubing in the borehole, and the lysimeters were placed under negative pressure to enhance flow from the surrounding unsaturated media into the ceramic sampling cups (Baker et al., 2004).

Tracer samples were returned to the Los Alamos National Laboratory, New Mexico, for analysis. Samples were analyzed for fluorobenzoates (FBAs) using high-performance liquid chromatography with UV absorbance detection and for Br using ion chromatography with conductivity detection. The quantification limit (QL) for Br and for 2,4-DFBA was 0.016 mg L^{-1}. Two QLs are shown for 2,4,5-TFBA; the samples from test 1 were run using a method with a QL of 0.008 mg L^{-1}, whereas the 2,4,5-TFBA analyses in samples that also contained 2,4-DFBA from test 2 had a QL of 0.024 mg L^{-1}. In some of the FBA plots (Fig. 4), data below the QL are shown; these data are included to provide a visual continuation of the breakthrough curve (BTC) and should not be considered to be quantitative. Only the FBA data are presented in this paper.

Tracer Test and Model Results

Breakthrough Curves

Collection of grab samples after the introduction of tracer to the south pond (Test 1) enabled coarse mapping of the spatial distribution of the tracer during infiltration. Tracer concentrations were highest in the northern third of the pond adjacent to the injection point. In the southeastern part of the pond, tracer concentrations were approximately one-third of those toward the north. The southwestern quadrant remained dry throughout the test. Tracer concentration in all portions of the pond dropped below the QL (0.016 mg L^{-1}) within the first 2 h after tracer was introduced to the pond.

The tracer tests yielded BTCs that provided information regarding transport through the alluvium, the alluvium–basalt complex, and the CD interbed for a range of vertical and lateral distances (Fig. 4). Test 1 data represent travel under quasi-steady-state flow conditions with considerable antecedent wetness. In contrast, the second tracer test BTCs represent transport under transient flow conditions arising from infiltration into an initially dry shallow system with relatively wet conditions at the contact between the basalt and the CD interbed. Initial and peak arrival times together with peak tracer concentrations are summarized in Table 2.

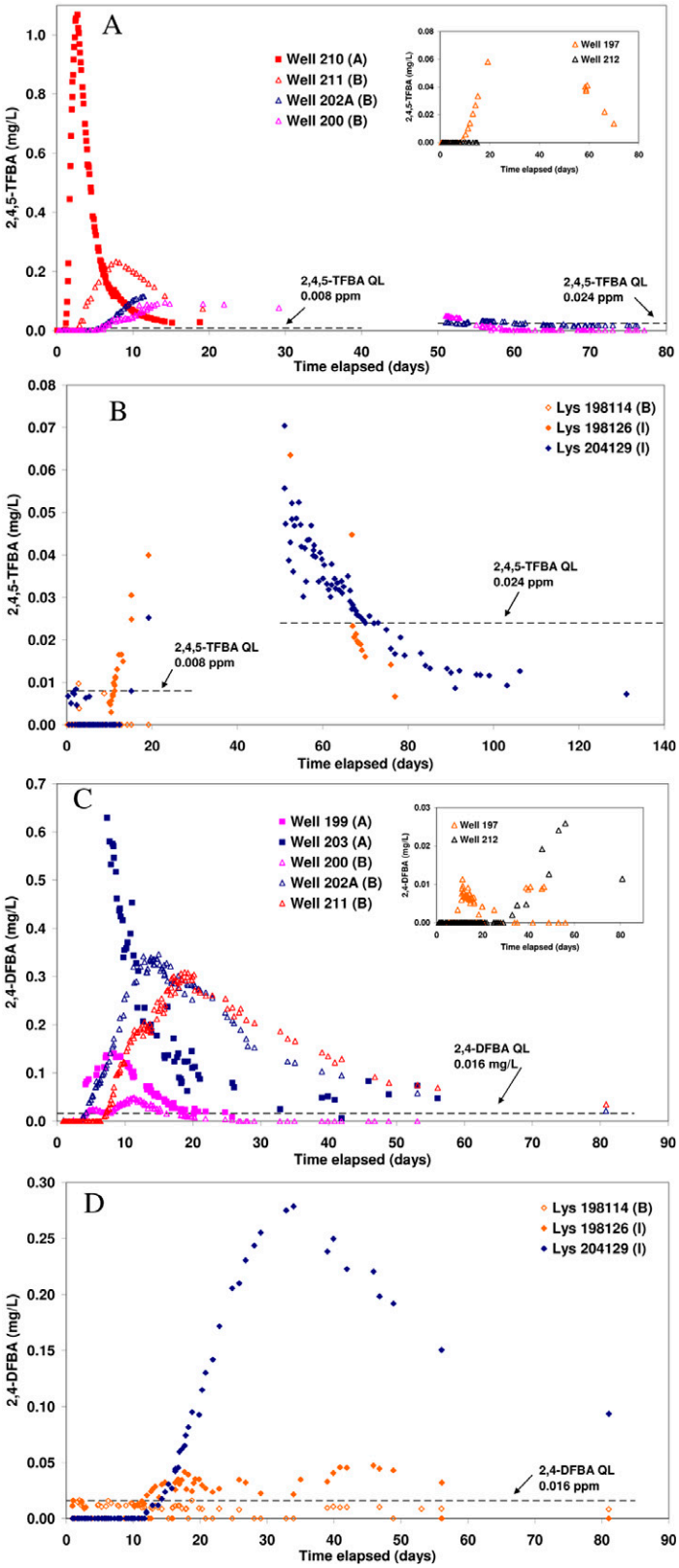

FIG. 4. Test 1 and test 2 breakthrough curves from wells and lysimeters (QL = analytical quantification limit).

Estimated Flow Velocities

The breakthrough curves generated at the VZRP were fitted using the one-dimensional advection–dispersion equation (1-D ADE) to yield estimates of flow velocity (v) for the alluvium, the integrated alluvium–basalt complex, and the CD interbed (Table 3). The CXTFIT code (Parker and van Genuchten, 1984; Toride et al., 1999) was used to fit breakthrough data with analytical solutions to the deterministic, equilibrium advection–dispersion equation:

TABLE 2. Summary of breakthrough behavior in tests 1 and 2.

Test 1			
Well ID	First arrival	Peak arrival	Peak 2,4,5-TFBA concentration
	d		mg L^{-1}
210(A)	1	2.7	1.1
197(B)	9	N/A†	N/A
200(B)	5	14	0.1
202A(B)	5	12	0.12
211(B)	3	8	0.25
212	29‡	N/A	N/A
Lysimeter ID			
198114(B)	27	N/A	N/A
198126(I)	21	35§	N/A
204129(I)	19	20–50	N/A

Test 2			
Well ID	First arrival	Peak arrival	Peak 2,4-DFBA concentration
	d		mg L^{-1}
199(A)	4¶	8	0.14
203(A)	6#	6–7††	>0.63
197(B) peak 1‡‡	N/A	10–20	0.011
197(B) peak 2	N/A	40–50	0.009
200(B) peak 1§§	3	5	0.025
200(B) peak 2	N/A	11	0.05
202A(B)	4	14	0.35
211(B)	7	19	0.31
212	46	N/A	N/A
Lysimeter ID			
198114(B)	27	N/A	N/A
198126(I)	17	N/A	N/A
204129(I)	12	34	0.28

† N/A Data not available.
‡ First arrival based on three data points all below quantification limit.
§ From interpolation between available data.
¶ First arrival based on water level data in well (Baker et al., 2004).
# First arrival based on water level data in well (Baker et al., 2004).
†† Peak arrival estimated from breakthrough curve slope.
‡‡ All 2,4-DFBA data below quantification limit, breakthrough curve bimodal.
§§ Well 200(B) breakthrough curve bimodal–presented in two peaks.

$$\frac{\partial C}{\partial t} = D_L(\theta)\frac{\partial^2 C}{\partial x^2} - v(\theta)\frac{\partial C}{\partial x} \quad [1]$$

where C is solute concentration (mg L^{-1}), D_L is longitudinal dispersion coefficient (m^2 d^{-1}), v is average pore water velocity, θ is volumetric water content, t is time (d), and x is transport distance (m).

The purpose of this modeling was to determine average flow velocities through different portions of the profile. For this exercise the volumetric water content within each unit was assumed to be constant, and Eq. [1] was simplified to

$$\frac{\partial C}{\partial t} = D_L\frac{\partial^2 C}{\partial x^2} - v\frac{\partial C}{\partial x} \quad [2]$$

Equation [2] describes transport of a nonreactive solute through a homogeneous porous medium under steady-state flow conditions. The initial and boundary conditions used in this study are

$$C(x, 0) = 0,\ t \geq 0$$

$$C(0, t) = C_0,\ 0 < t \leq t_0$$

$$C(0, t) = 0,\ t > t_0$$

$$\frac{\partial C}{\partial x}(\infty, t) = 0,\ t \geq 0$$

TABLE 3. Summary of flow velocities for both tracer tests.

Well identifier	Domain sampled		Travel distance†	v	R^2 ‡
			m	m d^{-1}	
		Test 1			
210(A)	Alluvium	max.	145	41	0.975
		min.	85	24	0.975
202A(B)	Alluvium/basalt	max.	166	8	0.971
		min.	124	6	0.971
211(B)	Alluvium/basalt	max.	157	13	0.996
		min.	97	8	0.996
		Test 2			
199(A)	Alluvium		136	13	0.955
200(B) peak 1	Alluvium/basalt		129	20	0.858
200(B) peak 2	Alluvium/basalt		129	10	0.939
202A(B)	Alluvium/basalt		131	5	0.981
211(B)	Alluvium/basalt		194	6	0.960
Lys 204129(I)	Alluvium/basalt/interbed		146	3	0.980

† See text for travel distance calculation.
‡ Coefficient of determination.

Initial time (t_0) is the time at which tracer was added to the system (and, for test 2, the time at which flow to the north pond was initiated). Tracer transport distance (x) is the sum of the horizontal and vertical components of flow (see below for further discussion). The constant concentration boundary condition was used despite the decreasing concentration over the 2 h that it took for tracer to infiltrate from the surface. We consider the error introduced by this departure from the defined boundary condition to be negligible because the rise and fall in concentration was relatively steep and the total infiltration time (~2 h) was short relative to the transport times (days to weeks). Thus, the injection approximated a pulse input. Total mass was included as a fitting parameter in the estimation procedure because the solute mass entering any given subset of flow pathways was not known. The only other parameters optimized were flow velocity (v) and dispersion coefficient (D_L).

The analytical model used in this work does not explicitly account for the complexity of transport through a geologically heterogeneous and variably saturated system. However, the model fits to the first arrival and peak portions of the BTCs are very good (Fig. 5), suggesting that although the geometry and flow conditions are oversimplified, the model provides reasonable overall estimates of average flow velocities in the system. In this paper, we use the estimates of flow velocities generated using the 1-D ADE to provide information on relative flow and transport between lithologic units under varying infiltration conditions. Dispersion coefficients are not reported as they are particularly sensitive to the fact that the test boundary conditions together with the transient, three-dimensional nature of the flow system violate many of the assumptions inherent in the 1-D ADE.

To determine transport velocities, travel distances must be estimated. In test 1, tracer was added to the south pond and is known to have distributed unevenly across the wetted area of the pond. On the basis of tracer concentrations measured in the pond and visual estimates of pond water volume, we assumed that most of the tracer mass infiltrated between the southeastern part of the pond, where water volume was greatest and near the discharge, where tracer concentrations were greatest. We recognize that due to the spreading of the tracer across the pond, possible travel distances encompass a wide range. To provide bounding estimates of flow velocity, model fits were performed assum-

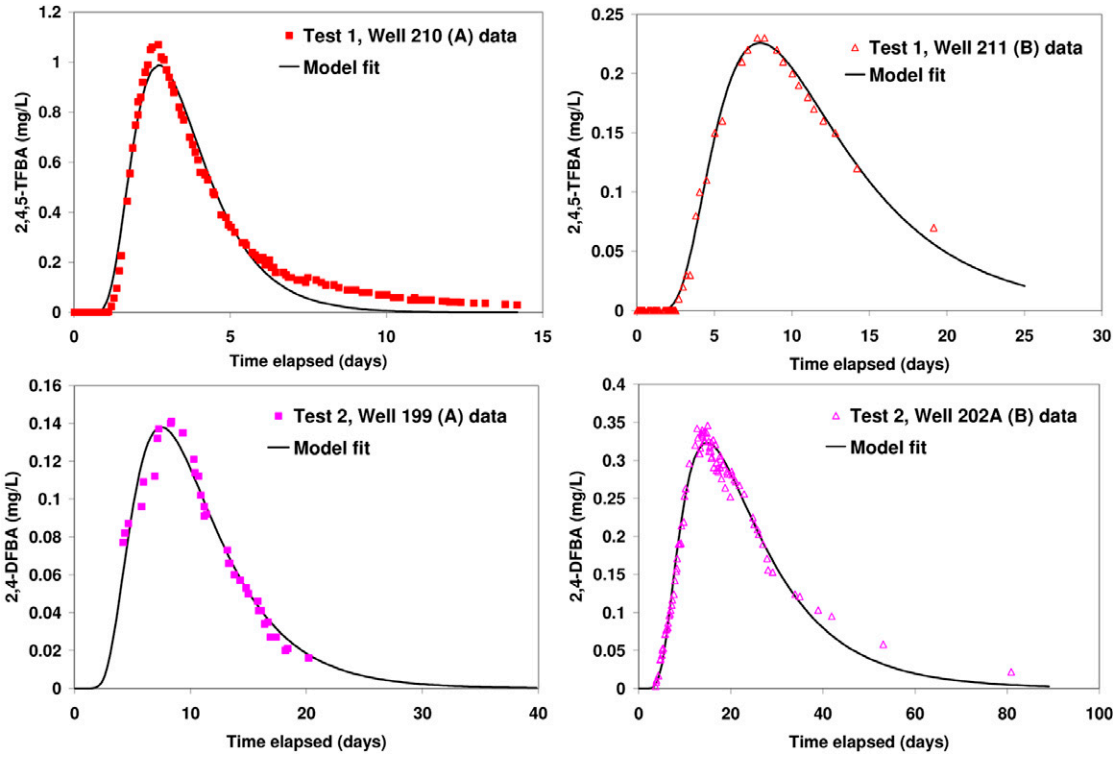

FIG. 5. Representative fits of test 1 and test 2 data from which flow velocity estimates were generated. See Table 3 for minimum and maximum transport distances used in these simulations.

ing two infiltration points, one in the southern part of the south pond and one at the discharge to the south pond. Maximum and minimum linear transport distances were calculated as the sum of the horizontal distance from each of these infiltration points to a given sampling location plus the depth to that sampling location. Three test 1 BTCs were fitted: one [well 210(A)] provides transport parameters for the alluvium, and two [wells 202A(B) and 211(B)] provide transport parameters for the integrated alluvium–basalt complex (Table 3). Model fits of a representative alluvial well [210(A)] and deeper well [211(B)] are shown in Fig. 5.

The estimated minimum and maximum flow velocities yielded by well 210(A) are 24 and 40 m d^{-1}, respectively. These velocities are integrated values for transport from the ponded water at the surface, down through the alluvium, and along the alluvium–basalt contact to the well. The minimum and maximum flow velocities estimated from BTCs in well 202A(B) are 6 and 10 m d^{-1}, and for well 211(B) are 8 and 13 m d^{-1}, respectively. In both cases, these represent integrated velocity distributions from several subdomains, which include flow across the alluvium–basalt contact, through the variably saturated basalt, and along the basalt–interbed contact.

In test 2, the tracer input was constrained to a shallow pool roughly 4 m in diameter within the north pond, so the tracer input signal was considered to be a point source. Maximum linear transport distances were calculated as the sum of the horizontal distance from the center of the tracer pool to the well and the depth of the well. This method yields an estimated maximum travel distance and thus provides an upper bound on the average linear velocity. Test 2 yielded four BTCs complete enough to be analyzed using CXTFIT; one alluvial well [well 199(A)] and three wells finished above the CD interbed [wells 200(B), 202A(B), and 211(B)]. Model fits of a representative alluvial well [199(A)] and deeper well [202A(B)] are shown in Fig. 5. Table 3 contains a summary of the velocity estimates from each BTC.

Discussion

Flow and Transport through the Surficial Alluvium

The alluvium at the VZRP, and throughout the ESRP, is known to be heterogeneous with gravel, sand, and clay layers and lenses interspersed throughout (Smith, 2004). In such a system, it is necessary to define a characteristic length scale below which the heterogeneity must be explicitly accounted for and above which effective properties (e.g., hydraulic conductivity) may be used to represent the system as a whole (Bear, 1972). According to the current conceptual model, flow through the surficial alluvium is expected to be largely vertical until the alluvium–basalt contact is reached and lateral spreading occurs. Flow pathways along the alluvium–basalt contact to the north and northwest are intercepted by two shallow wells [199(A) and 203(A)]. To assess transport behavior through the alluvium at the scale of the tracer tests, a forward simulation was performed using the tracer travel distance for well 203(A) during test 2 (122 m) together with the velocity and dispersion coefficient generated from an inverse fit of the test 2 well 199(A) BTC. The results of the forward simulation were compared with the BTC from well 203(A) (Fig. 6). The 1D-ADE with v and D from well 199(A) provides a reasonable estimate of the position of the peak and predicts all but the very late-time tailing behavior in well 203(A). That one set of transport parameters describes breakthrough behavior in both wells suggests that, despite the known heterogeneity of the porous medium, comparable transport pathways through the alluvium formed to the north and the northwest. This in turn suggests that transport distances more than ~15 m vertically and ~100 m laterally are greater than the characteristic length for this medium.

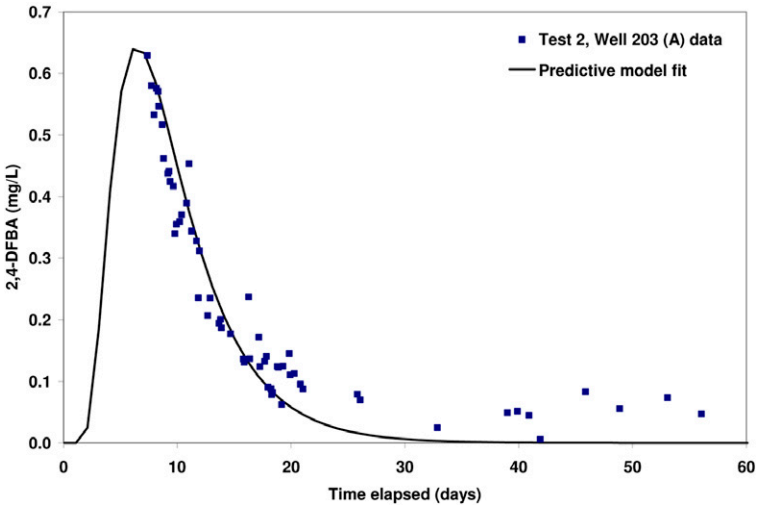

FIG. 6. Prediction of test 2 well 203(A) data using parameters from an inverse fit of test 2 well 199(A) breakthrough curve.

Flow and Transport across the Alluvium–Basalt Contact

The behavior of the alluvial wells suggests that although a saturated layer forms at the alluvium–basalt contact, providing a mechanism for some horizontal transport, this perched layer is neither laterally extensive nor temporally persistent. In test 1, only well 210(A) at the south end of the south pond produced water; the other two alluvial wells [199(A) and 203(A)] were dry. When discharge was switched from the south pond to the north pond, well 210(A) dried up within 4 d and wells 199(A) and 203(A) began producing water within 4 to 6 d. Water never reached well 196(A), an alluvial well farther to the north of the north pond (~228 m from well 212). This behavior strongly suggests that vertical flow across the alluvium–basalt contact is sufficiently large to limit the extent of lateral flow along the contact. In addition, significant tracer masses were recovered at the deeper wells in the same well clusters as the alluvial wells. Both of these observations are inconsistent with the alluvium–basalt contact acting as a lateral conduit to move a significant portion of the infiltrating water out of the monitoring domain of the VZRP. Rather, it appears that perched zones that form at the alluvium–basalt contact do not extend far beyond the margins of surface source and drain within days after the source of infiltration is removed. Other studies based on monitoring at both the RWMC and the INTEC support this conclusion (Cecil et al., 1991; Hull and Bishop, 2003). This result is important as it shows that perched water at the alluvium–basalt contact cannot store a large amount of water or solute, move water or solute over laterally extensive distances, or significantly retard the downward movement of water or potential contaminants.

Flow and Transport through the Basalt

The results of our tracer tests indicate that during high-intensity infiltration from the surface into unsaturated basalt, flow occurred primarily in the fractures. In test 2, three BTCs [wells 197(B) and 200(B) and lysimeter 198126(I); Fig. 4] are bimodal, supporting the idea that miscible displacement as conceptualized in porous media does not apply to flow in the fractured basalt of the ESRP. The most plausible explanation for compound BTCs is that flow occurred along multiple flow paths with different flow lengths and/or flow velocities (Mohanty et al., 1998; Nimmo et al., 2002).

Flow velocities through the alluvium–basalt complex range from ~5 to ~20 m d^{-1} (Table 3). If flow was matrix dominated, we would expect flow velocities on the order of 0.4 m d^{-1} based on the laboratory-measured mean vertical saturated hydraulic conductivity for ESRP basalt matrix (saturated hydraulic conductivity, K_{sat}, = 8.4 × 10^{-2} m d^{-1}; Bishop, 1991). The velocities observed in the field are one to two orders of magnitude greater than can be explained by matrix flow alone. We interpret the evidence of multiple flow paths, together with high flow velocities, as indicating that flow through the basalt occurred primarily in the fractures even when the matrix was unsaturated.

Flow and Transport through the Sedimentary Interbeds

The sedimentary interbeds in the ESRP vadose zone are thought to exert important controls on flow and transport, both physically and chemically. The formation of perched zones above the major sedimentary interbeds indicates that the interbeds act as barriers to vertical flow as well as facilitating lateral flow along the basalt–interbed contact (Newman and Dunnivant, 1995; Nimmo et al., 2002; Wood and Norrell, 1996). In current conceptual and numerical models of flow and transport in the ESRP vadose zone, sorption of contaminants is assumed to occur only within the surficial sediment and the sedimentary interbeds (Magnuson and Sondrup, 2006). Clearly, the higher sorptive capabilities of these sediments may only be called on if in fact flow patterns result in significant sediment–water interaction. Thus, it is important to understand whether vertical flow occurs via percolation through the sedimentary material of the interbeds or if preferential flow paths such as high conductivity channels within the interbeds or interbed discontinuities result in significant bypassing of the interbed material.

By analyzing tracer BTCs collected above and below the CD interbed, flow velocities were calculated for the sedimentary interbed and associated clay-filled, fractured basalt. The computed velocities were compared with velocities calculated from laboratory-derived sediment characteristics, the results of a water-balance calculation, and breakthrough behavior in a deep well at the VZRP to investigate the nature of flow through the interbed. Pore water pressure data from the tensiometer at 38.7 m in borehole 204 indicated that the CD interbed saturated quickly in response to infiltration from the VZRP ponds and remained saturated during both tracer tests (Baker et al., 2004).

Figure 7 shows 2,4-DFBA BTCs at well 202A(B) and lysimeter 204129(I). This well and lysimeter are in the same nested set located to the northwest of the northern VZRP pond. Well 202A(B) is completed in a basalt rubble zone just above the CD interbed (the well is screened between 35.8 and 37.3 m bls, and sedimentary interbed material was encountered at a depth of 37.5 m bls). Lysimeter 204129(I) is installed within the CD interbed at a depth of 39.3 m bls. Given that the lateral flow distances from the tracer injection point to well 202A(B) and borehole 204 are similar (107 m and 120 m from well 212, respectively; see Table 1), the tracer breakthrough at well 202A(B) is assumed to be representative of the tracer arrival above the interbed in borehole 204. Thus, the distribution of tracer at 202A(B) was

used as an input signal to fit the BTC at 204129(I) and calculate the flow velocity through the sedimentary interbed and clay-filled fractured basalt. This analysis yielded an estimated flow velocity of 0.12 m d^{-1}.

To address the question of whether preferential flow paths allow significant bypassing of the sedimentary interbeds, it is informative to compare the hydraulic conductivity values derived from the results of inverse modeling with values calculated using laboratory hydraulic parameters. Comprehensive characterization of the VZRP interbed sediments has yielded estimates of saturated hydraulic conductivity (K_{sat}) in the interbed materials (USDOE-ID, 2006; Winfield, 2003). Hydraulic conductivity values for the CD interbed range over four orders of magnitude (10^{-5} to 10^{-1} m d^{-1}), decrease with depth, and have a mean value of 5.76×10^{-2} m d^{-1}. The average porosity for the CD interbed is 0.496 (Winfield, 2002). The mean water level above the upper boundary of the CD interbed for the duration of the second tracer test was 3.16 m. A Darcy calculation using a pressure head of 3.16 m, a flow velocity of 0.12 m d^{-1}, a vertical transport distance of 1.98 m and porosity of 0.496 yields a saturated hydraulic conductivity of $\sim 2 \times 10^{-2}$ m d^{-1}. Clearly, the interbeds are highly heterogeneous with respect to K_{sat}; however, the field-derived flow velocity yields an estimated value for K_{sat} that is very close to the mean laboratory-derived K_{sat} value (both on the order of 10^{-2} m d^{-1}). This agreement between laboratory- and field-derived transport parameters lends credence to the hypothesis that vertical flow occurs through the main bulk of the sedimentary material of the CD interbed.

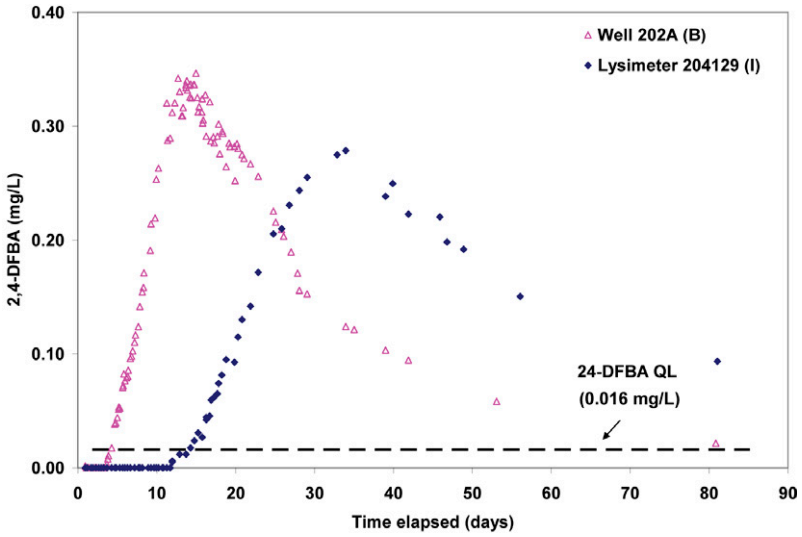

FIG. 7. Test 2 breakthrough curves for well 202A(B) and lysimeter 204129(I).

A simple water-balance calculation was used to estimate the saturated vertical hydraulic conductivity of the CD interbed on a larger scale than that interrogated by the preceding analysis. Assuming that water moves predominantly vertically from the surface and then spreads radially along the CD interbed, the rate at which water percolates vertically through the interbed controls the extent to which the perched water spreads. During test 1, water reached well 197(B), located ~268 m from the center of the south pond, but failed to reach well 194(B), located ~449 m from the center of the south pond (Fig. 2). These two wells provide bounding estimates of the radial distance that water traveled along the CD interbed and thus of the area of the circles through which water percolated vertically. Darcy calculations using the two bounding areas (2.3×10^5 and 6.3×10^5 m^2) yielded estimates of vertical saturated hydraulic conductivity for the CD interbed of 8×10^{-3} and 3×10^{-3} m d^{-1}, respectively. The fact that these values are so close to both the estimate based on the well 202(A), lysimeter 204129(I) analysis (2×10^{-2} m d^{-1}) and the mean laboratory value (5.76×10^{-2} m d^{-1}) suggests that the interbed (i) is laterally continuous over an extensive area, (ii) does not contain significant high-permeability vertical channels, and (ii) is homogeneous enough that its large-scale effective vertical permeability is represented quite well by averaged point measurements

Analysis of tracer breakthrough in well 212 can also be used to further our investigation into the nature of transport through the vadose zone. Well 212 is completed at a depth of 79 m bls and is located between the two ponds almost directly below the infiltration point (Fig. 2). The well penetrates a total of 8 m of sedimentary material and ~1 m of clay-filled fractured basalt distributed in four separate interbeds. Cement grout and bentonite plugs from land surface to approximately 2 m above the screened interval prevents vertical flow down the annulus of the well. Transport through the ESRP vadose zone to the regional aquifer can be conceptualized in terms of two end members. The first of these is that water moves primarily through the fractured basalt, traveling laterally along the tops of the sedimentary interbeds until a gap is found. The second end member is that vertical transport rates are predominantly controlled by transport through the sedimentary material of the interbeds and associated clay-filled fractures in the basalt. Presumably, the true transport paths lie between these two extremes. To assess the nature of flow paths through the interbeds, two forward simulations were performed and compared with the test 2 data from well 212 (Fig. 8). In both simulations, lateral flow is not included as lateral flow velocities are rapid compared with vertical flow velocities (see next section for discussion of lateral flow along basalt–interbed contacts). In the first simulation, flow and transport are assumed to be predominantly through the basalt; that is, flow bypasses the sedimentary material and associated clay-filled fractures of the interbeds. In the second simulation, flow and transport are assumed to be through the sedimentary interbeds and associated basalt with clay-filled fractures with no bypassing. Since transport velocities through the basalt are roughly two orders of magnitude faster than those through the interbed (Table 3), flow through the basalt is neglected in simulation 2.

The forward simulations clearly show that transport parameters for the sedimentary material of the interbeds and the associated clay-filled fractured basalt best match the test 2 well 212 BTC (Fig. 8). The simulation in which the interbeds are neglected predicts initial arrival of tracer in well 212 ~25 d too early. This simulation also predicts a very steep rising limb of the BTC whereas the data show a slower, shallower rise in tracer concentrations. The results of simulation 2 provide a much closer match to the well 212 data with an initial arrival time of ~40 d. This result indicates that most of the tracer that arrived at well 212 likely traveled through the interbeds. The

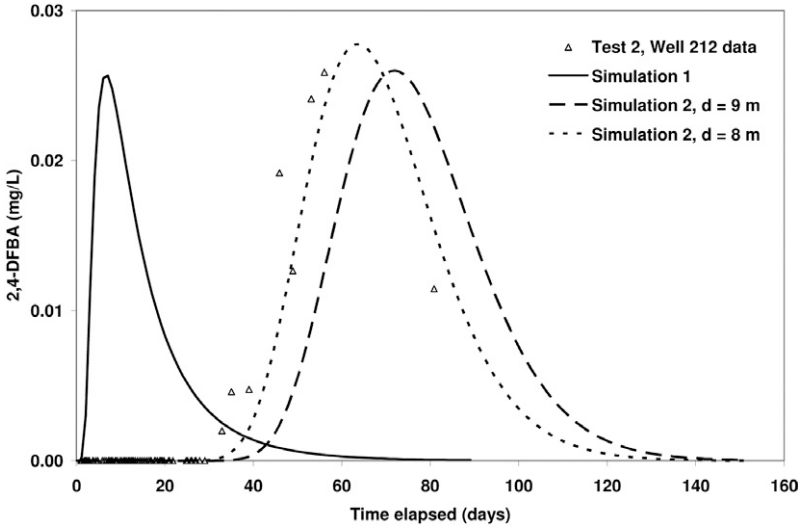

FIG. 8. Results of CXTFIT simulations compared with test 2 well 212 breakthrough data (see text for conceptual model in each simulation); d = effective interbed thickness.

simulated breakthrough is somewhat later than that observed in well 212; however the fit is considerably improved by decreasing the assumed effective interbed thickness to 8 m instead of 9 m. Although the difference between an effective interbed thickness of 8 and 9 m is small considering the uncertainties inherent in this analysis, the improved fit using the smaller number does allow the possibility that some flow may bypass the interbed material. Other possibilities that could account for this relatively small difference between predicted and measured interbed thicknesses without any bypassing include spatial variability of interbed thickness surrounding well 212, locally higher heads due to variable perched water thickness above the CD interbed or other interbeds penetrated by well 212, and heterogeneity in hydraulic conductivity both within and between the CD interbed and the deeper interbeds.

Comparison of field-derived hydraulic conductivity values with those generated in the laboratory, together with a simple model analysis of tracer breakthrough at a deep well, provides strong evidence that solutes move through both the sedimentary material and the associated clay-filled fractures in the basalt during vertical transport. A small degree of bypassing is allowed by the data but not required given the uncertainties inherent in this analysis and the likely variable thicknesses and heterogeneous characteristics of the interbed materials. This finding has important implications for contaminant transport as retardation of reactive solutes is expected to be much higher in sedimentary material and clay-filled fractures than in the basalt alone (Magnuson and Sondrup, 2006).

Lateral Transport along the Basalt–Interbed Contact

When water infiltrating vertically through the variably saturated basalt reaches a sedimentary interbed, it forms a perched layer. From this perched layer water is redistributed both vertically through and laterally along the interbed. Tracer recovery at well 200(B) and at well 197(B) (Fig. 2 and 3) may be used to provide insight into the lateral component of this flow. Well 200(B) is completed above the upper boundary of the CD interbed slightly to the north of the north pond. Well 197(B) is similarly completed above the CD interbed approximately 86 m due north of well 200(B). A Darcy calculation was performed using a hydraulic gradient based on water levels in wells 200(B) and 197(B), tracer arrival times at the two wells, and an assumed porosity of 0.5 (a reasonable assumption for both CD interbed [Winfield, 2002] and the basalt rubble zone [Smith, 2004]). If flow from well 200(B) to well 197(B) is assumed to be linear in nature, this calculation yields an estimated mean K_{sat} of $\sim$500 m d^{-1}; if a radial flow assumption is made, the calculated value is $\sim$900 m d^{-1}. Nimmo et al. (2004b) stated that the saturated hydraulic conductivity of basalt rubble zones is likely similar to that of gravel and could easily exceed 800 m d^{-1}. In contrast, the mean vertical saturated hydraulic conductivity of the CD interbed as determined by Winfield (2003) is 5.76×10^{-2} m d^{-1}, and tracer breakthrough analysis presented above yields a comparable value of 2×10^{-2} m d^{-1}. Even allowing for the possibility that the sedimentary materials of the interbed have high horizontal to vertical anisotropy in hydraulic conductivity, this large contrast in K_{sat} values strongly suggests that lateral flow occurred in the basalt rubble above the CD interbed rather than within the sedimentary material itself.

Perching Behavior at Different Geologic Contacts

Perching behavior at the alluvium–basalt contact differs significantly from that which occurs at the basalt–interbed contact. Although a saturated layer did form at the alluvium–basalt contact, it was not persistent once the source of water from the surface was discontinued. In contrast, the perched layer that formed at the basalt–interbed contact remained stable even after the source was moved between ponds. The perched water at the alluvium–basalt contact did not extend far beyond the wetted footprint at the surface, whereas the perched layer that formed at the basalt–interbed contact extended well beyond the surface infiltration source clearly indicating significant lateral flow (on the order of 100s of meters). This dissimilarity in perching behavior suggests that the perching mechanisms at the two contacts are different. We suggest that when unconsolidated material overlies fractured rock (as typified by the alluvium–basalt contact), the underlying rock functions as a capillary barrier and water moves into the basalt when the head above the contact exceeds the air-entry pressure of the transmissive fractures. In contrast, the thicker, more extensive perching at the basalt–interbed contact is likely due to the permeability contrast between the fractured rock and the relatively low permeability interbed sediments.

Comparison of Flow Velocities in Test 1 and 2

Flood events in semiarid systems occur on a variety of temporal scales. For example, at INL, infiltration from the Big Lost River and associated spreading areas may continue for months or years, whereas local snowmelt and rainfall may cause intense infiltration events that last from days to weeks. These two temporal scales are simulated by test 1 and test 2. Test 1 was conducted after water had been infiltrating for roughly 9 mo. In contrast, test 2 was conducted in an initially dry setting and the test duration was approximately 2 mo. Flow velocities calcu-

lated for test 1 are consistently faster than those calculated for test 2 (Table 3).

Two fundamental differences between test 1 and test 2 are the antecedent wetness and the location of the infiltration points. That tests 1 and 2 were performed in separate ponds allows the possibility that differences in flow velocities are due to flow through different pathways. In such a case, however, one would also expect that there would be a distribution of flow velocities and that each different infiltration location would produce some slower and some faster pathways. There is no a priori reason to expect that flow paths from one pond would give rise to consistently higher flow velocities than another. Rather, the consistent trend of faster flow velocities in test 1 suggests that system wetness is an important controlling factor in both the basalt and the alluvium. This correlation is presumably related to increased unsaturated hydraulic conductivity associated with increased moisture content. In addition, once the flow field approaches steady state, flow velocities in the fractured basalt may be higher due to the presence of saturated or near-saturated fractures that are able to act immediately as transmissive pathways. This interpretation suggests that during long-term infiltration events, velocities in the alluvium may be as much as a factor of two to three higher than during initial infiltration into a dry system. Similarly, flow through the alluvium/basalt complex may be expected to be 50 to 100% faster under wetter antecedent conditions. Thus, the relative difference in flow velocities calculated for test 1 and test 2 may be useful in evaluating contaminant transport under temporally different infiltration scenarios.

Conclusions

The work outlined in this paper provides evidence that when driven by high-flux infiltration from the surface, flow occurs in fractures even when matrix saturations are low. This fracture flow gives rise to vertical transport rates that are much higher than would be predicted assuming that the flow occurs primarily in the matrix. Vertical flow velocities through the combined surficial alluvium and fractured basalt at the VZRP were determined to range between 5 and 20 m d^{-1}. Flow velocities were 50 to 100% faster under quasi-steady-state conditions with higher antecedent wetness than they were when infiltration occurred under initially dry and highly transient conditions. This increase in flow rates is presumed to result from higher unsaturated hydraulic conductivities related to higher moisture contents. In addition, we propose that under steady-state conditions, flow velocities increase because fractures are already behaving as active transmissive pathways, in contrast to the transient case in which the fractures must go through an initial wetting-up phase.

Perching and flow behavior at two types of geologic contacts were investigated during this study: the contact between the surficial alluvium and the underlying basalt and the contact between basalt and a sedimentary interbed. The dissimilarity in perching behavior suggests a fundamental difference in the perching mechanism at the two contacts. We propose that when unconsolidated sediment overlies fractured rock, the underlying rock presents a capillary barrier, with water moving vertically into the rock only when the head above the contact exceeds the air-entry pressure of the fractures. In contrast, when fractured rock overlies sedimentary material, perching appears to be due to the contrast in permeability between the high-permeability fractured rock and the relatively low-permeability interbed sediments. This is an important distinction as the capillary barrier mechanism is head-dependent and may therefore give rise to pulsing or flushing of flow across the contact, whereas the permeability-controlled mechanism is independent of head above the contact and is therefore a permanent feature of the subsurface environment.

Water perched above the CD interbed flowed laterally and also percolated vertically through the sedimentary material of the interbed. Results of our tracer tests suggest that lateral flow along the basalt–interbed contact occurs in a high-permeability, high-porosity zone, perhaps of basalt rubble, that lies above the sedimentary interbed. The mean saturated hydraulic conductivity of this zone is estimated to be on the order of either 500 or 900 m d^{-1} for lateral and radial flow assumptions, respectively. Vertical flow occurs through the sedimentary material of the interbeds with little or no apparent bypassing of the interbed through preferential pathways. The estimated mean vertical saturated hydraulic conductivity of CD interbed sediments based on analysis of flow at a single point is $\sim 2 \times 10^{-2}$ m d^{-1}; a larger scale analysis yielded bounding values of 3×10^{-3} and 8×10^{-3} m d^{-1} for infiltration through an interbed area of $\sim 10^5$ m^2.

Acknowledgments

This work was supported by the Environmental Management Science Program of the Office of Science, U.S. Department of Energy. We would like to thank Leah Street and her crew for great operational support in the field at INL. In addition, we would like to thank Dr. John Nimmo and two anonymous reviewers for very thorough reviews that greatly improved this paper.

References

Ackerman, D.J. 1991. Transmissivity of perched aquifers at the Idaho National Engineering Laboratory, Idaho, Water-Resources Investigations Report 91-4114. USGS, Idaho Falls, ID.

Adam, M.L., S.D. Comfort, M.C. Morley, and D.D. Snow. 2004. Remediating RDX-contaminated ground water with permanganate: Lab. investigations for the Pantex perched aquifer. J. Environ. Qual. 33:2165–2173.

Anderson, S.R., and B.D. Lewis. 1989. Stratigraphy of the unsaturated zone at the radioactive waste management complex, Idaho National Engineering Laboratory, Idaho. Water Resources Investigations Report 89-4065. USGS, Idaho Falls, ID.

Baker, K.E., L.C. Hull, J. Bennett, S.L. Ansley, and G. Heath. 2004. Conceptual models of flow through a heterogeneous, layered vadose zone under a percolation pond, INEEL/EXT-04-01679. Idaho National Engineering and Environmental Lab., Idaho Falls, ID.

Barraclough, J.T., J.B. Robertson, and V.J. Janzer. 1976. Hydrology of the solid waste burial ground, as related to the potential migration of radionuclides. Idaho National Engineering Lab. Open File Report 76-471. USGS, Idaho Falls, ID.

Bear, J. 1972. Dynamics of fluids in porous media. Elsevier, New York.

Bishop, C.W. 1991. Hydraulic properties of vesicular basalt. Master's thesis, Univ. of Arizona.

Cecil, L.D., B.R. Orr, T. Norton, and S.R. Anderson. 1991. Formation of perched ground-water zones and concentrations of selected chemical constituents in water, Idaho National Engineering Laboratory, Idaho, 1986–1988. Water Resources Investigations 91-4166, DOE/ID-22100. USGS, Idaho Falls, ID.

USDOE-ID. 2006. Operable unit 3-14 tank farm soil and groundwater remedial investigation/baseline risk assessment. DOE/NE-ID-11227, Rev. 0. USDOE, Idaho Operations Office, Idaho Falls.

Doughty, C. 2000. Numerical model of water flow in a fractured basalt vadose zone: Box Canyon site, Idaho. Water Resour. Res. 36:3521.

Dunnivant, F.M., M.E. Newman, C.W. Bishop, D. Burgess, J.R. Giles, B.D.

Higgs, J.M. Hubbell, E. Neher, G.T. Norrell, M.C. Pfiefer, I. Porro, R.C. Starr, and A.H. Wyllie. 1998. Water and radioactive tracer flow in a heterogeneous field-scale system. Ground Water 36:949–958.

Dunnivant, F.M., M.E. Newman, S.O. Magnuson, and J. McCarthy. 1995. Modeling of radioactive tracer data collected during the large-scale pumping and infiltration test: Water velocity and dispersivity estimates. EOS Trans. 76, Suppl., 266.

Fabryka-Martin, J., S.J. Wightman, W.J. Murphy, M.P. Wickham, M.W. Caffee, G.J. Nimz, J.R. Southon, and P. Sharma. 1993. Distribution of chlorine-36 in the unsaturated zone at Yucca Mountain: An indicator of fast transport paths. *In* Proc. FOCUS '93, Site Characterization and Model Validation, American Nuclear Society, Las Vegas, NV. 17–21 Sept. 1993. American Nuclear Society, La Grange Park, IL.

Fabryka-Martin, J., S.J. Wightman, B.A. Robinson, and E.W. Vestal. 1994. Infiltration processes at Yucca Mountain inferred from chloride and chlorine-36 distributions. Milestone Report 4317. Los Alamos National Lab., Los Alamos, NM.

Faybishenko, B., C. Doughty, M. Steiger, J.C.S. Long, T.R. Wood, J.S. Jacobsen, J. Lore, and P.T. Zawislanski. 2000. Conceptual model of the geometry and physics of water flow a fractured basalt vadose zone. Water Resour. Res. 36:3499–3520.

Finsterle, S., J.T. Fabryka-Martin, and J.S.Y. Wang. 2002. Migration of a water pulse through fractured porous media. J. Contam. Hydrol. 54:37–57.

Flint, A.L., L.E. Flint, G.S. Bodvarsson, E. Kwicklis, and J. Fabryka-Martin. 2001a. Evolution of the conceptual model of unsaturated zone hydrology at Yucca Mountain, Nevada. J. Hydrol. 247:1–30.

Flint, A.L., L.E. Flint, E.M. Kwicklis, G.S. Bodvarsson, and J.M. Fabryka-Martin. 2001b. Hydrology of Yucca Mountain, Nevada. Rev. Geophys. 39:447–470.

Gauthier, J.H., M.L. Wilson, and F.C. Lauffer. 1992. Estimating the consequences of significant fracture flow at Yucca Mountain. *In* Proc. Third Annu. Int. High-Level Radioactive Waste Management Conf., Las Vegas, NV. 12–16 Apr. 1992. American Nuclear Society, La Grange Park, IL.

Hull, L.C., and C.W. Bishop. 2003. Fate of brine applied to unpaved roads at a radioactive waste subsurface disposal area. Vadose Zone J. 3:190–202.

Illman, W.A., and D.L. Hughson. 2005. Stochastic simulations of steady state unsaturated flow in a three-layer, heterogeneous, dual continuum model of fractured rock. J. Hydrol. 307:17–37.

Liu, H.-H., C. Doughty, and G.S. Bodvarsson. 1998. An active fracture model for unsaturated flow and transport in fractured rocks. Water Resour. Res. 34:2633–2646.

Magnuson, S.O. 1995. Inverse modeling for field-scale hydrologic and transport parameters of fractured basalt. INEL-95/0637. Idaho National Engineering Lab., Idaho Falls.

Magnuson, S.O. 2004. Regulatory modeling for the Idaho National Engineering and Environmental Laboratory's Subsurface Disposal Area and conceptual model uncertainty treatment. Vadose Zone J. 3:59–74.

Magnuson, S.O., and A.J. Sondrup. 2006. Subsurface flow and transport model development for the operable unit 7-13/14 remedial investigation and feasibility study. ICP/EXT-05-01016. Idaho Cleanup Project, Idaho National Lab., Idaho Falls.

Mattson, E.D., S.O. Magnuson, and S.L. Ansley. 2004. Interpreting INEEL vadose zone water movement on the basis of large-scale field tests and long-term vadose zone monitoring results. Vadose Zone J. 3:35–46.

McLaren, R.G., P.A. Forsyth, E.A. Sudicky, J.E. VanderKwaak, F.W. Schwartz, and J.H. Kessler. 2000. Flow and transport in fractured tuff at Yucca Mountain: Numerical experiments on fast preferential flow mechanisms. J. Contam. Hydrol. 43:211–238.

Mohanty, B.P., R.S. Bowman, J.M.H. Hendrickx, J. Simunek, and M.T. van Genuchten. 1998. Preferential transport of nitrate to a tile drain in an intermittent-flood-irrigated field: Model development and experimental evaluation. Vadose Zone J. 34:1061–1076.

Montazer, P., and W.E. Wilson. 1984. Conceptual hydrologic model of flow in the unsaturated zone, Yucca Mountain, Nevada. Water Resources Investigation Report 84-4345. USGS, Lakewood, CO.

Newman, M.E., and F.M. Dunnivant. 1995. Results from the large-scale aquifer pumping and infiltration tests: Transport of tracers through fractured media. INEL-95/146 ER-WAG7-77. Idaho National Engineering and Environmental Lab., Idaho Falls.

Nimmo, J.R., K.S. Perkins, P.E. Rose, J.P. Rousseau, B.R. Orr, B.V. Twining, and S.R. Anderson. 2002. Kilometer-scale rapid transport of naphthalene sulfonate tracer in the unsaturated zone at the Idaho National Engineering and Environmental Laboratory. Vadose Zone J. 1:89–101.

Nimmo, J.R., K.S. Perkins, and K.A. Winfield. 2004a. Unsaturated-zone case study at the Idaho National Engineering and Environmental Laboratory: Can Darcian hydraulic properties predict contaminant migration? *In* Annu. Meeting, Geological Society of America, Denver, CO. 7–10 Nov. 2004. Geological Society of America, Boulder, CO.

Nimmo, J.R., J.P. Rousseau, K.S. Perkins, K.G. Stollenwerk, P.D. Glynn, R.C. Bartholomay, and L.L. Knobel. 2004b. Hydraulic and geochemical framework of the Idaho National Engineering and Environmental Laboratory vadose zone. Vadose Zone J. 3:6–34.

Parker, J.C., and M.T. van Genuchten. 1984. Determining transport parameters from laboratory and field tracer experiments. Bull. 84-3. Va. Agric. Exp. St., Blacksburg.

Peters, R.R., and E.A. Klavetter. 1988. A continuum model for water movement in an unsaturated fractured rock mass. Water Resour. Res. 24:416–430.

Pruess, K. 1999. A mechanistic model for water seepage through thick unsaturated zones in fractured rocks of low matrix permeability. Water Resour. Res. 35:1039–1051.

Rightmire, C.T., and B.D. Lewis. 1987. Hydrogeology and geochemistry of the unsaturated zone. Water Resources Investigations Report 87-4198. USGS, Radioactive Waste Management Complex, Idaho National Engineering Lab., Idaho Falls.

Robinson, B.A., D.E. Broxton, and D.T. Vaniman. 2005. Observations and modeling of deep perched water beneath the Pajarito Plateau. Vadose Zone J. 4:637–652.

Schaefer, C.J., and S.A. Kattenhorn. 2004. Characterization and evolution of fractures in low-volume pahoehoe lava flows, eastern Snake River Plain, Idaho. Geol. Soc. Am. Bull. 116, doi:10.1130/B25335.25332.

Smith, R.P. 2004. Geologic setting of the Snake River Plain aquifer and vadose zone. Vadose Zone J. 3:47–58.

Toride, N., F.J. Leij, and M.T. van Genuchten. 1999. The CXTFIT code for estimating transport parameters from laboratory or field tracer experiments. Research report no. 137. U.S. Salinity Lab., USDA, Riverside, CA.

Wang, J.S.Y., and T.N. Narasimhan. 1985. Hydrologic mechanisms governing fluid flow in a partially saturated, fractured, porous medium. Water Resour. Res. 21:1861–1874.

Wang, J.S.Y., and T.N. Narasimhan. 1993. Unsaturated flow in fractured porous media. p. 325–394. *In* J. Bear, C.-F. Tsang, and G. de Marsily (ed.) Flow and contaminant transport in fractured rock. Academic Press, San Diego, CA.

Winfield, K.A. 2002. Measurement of unsaturated hydraulic conductivity functions, saturated hydraulic conductivity, particle-size distribution bulk density, porosity, and specific surface area for Vadose Zone Research Park samples. Summary Report, USGS, Idaho National Engineering and Environmental Lab., Menlo Park, CA.

Winfield, K.A. 2003. Spatial variability of sedimentary interbed properties near the Idaho Nuclear Technology and Engineering Center at the Idaho National Engineering and Environmental Laboratory, Idaho. Water Resources Investigations Report 03-4142. USGS, Idaho Falls, ID.

Wood, T.R., and G.T. Norrell. 1996. Integrated large-scale aquifer pumping and infiltration tests: Groundwater pathways OU 7-06. Summary report INEL-96/0256. Idaho National Engineering and Environmental Lab., Idaho Falls.

Yang, I.C., G.W. Rattray, and P. Yu. 1996. Interpretations of chemical and isotopic data from boreholes in the unsaturated-zone at Yucca Mountain, Nevada. Water Resources Investigations Report 96-4058. USGS, Denver, CO.